Temperature- and Conformation-Dependent Luminescence of Benzanilides†

Frederick D. Lewis* and Weizhong Liu

Department of Chemistry, Northwestern University, Evanston, Illinois 60208-3113

Received: May 24, 2001; In Final Form: August 14, 2001

The luminescence of benzanilide, *N*-methylbenzanilide, and two cyclic analogues has been investigated as a function of temperature both in microcrystals and in the glass-forming solvent methyltetrahydrofuran. Potential energy surfaces for small-amplitude geometric relaxation of the excited states and large amplitude twisting about the amide bond in the ground and excited states have been explored using AM1 and RCIS calculations, respectively. ZINDO calculations have been used to probe the electronic configuration of the planar and twisted singlet and triplet states. Correlation of the spectroscopic and computational results indicates that at 77 K benzanilide phosphorescence occurs from a planar π,π^* triplet state whereas fluorescence occurs from a singlet state with partially relaxed geometry. At higher temperatures, large-amplitude geometric relaxation results in the formation of an intramolecular charge-transfer (TICT) state that is twisted about the amide C−N bond. This TICT state is responsible for the weak Stokes-shifted fluorescence observed from benzanilide and *N*-methylbenzanilide in fluid solution. Inhibition of amide twisting in cyclic derivatives precludes observation of TICT fluorescence.

Introduction

The luminescence of benzanilide (BA) and its derivatives continues to be the source of interest and conflicting interpretations.[1−8] At room temperature, BA is very weakly fluorescent ($\Phi_f < 10^{-3}$) in nonpolar solvents and nonfluorescent in polar solvents. No fewer than three fluorescent states have been identified by various workers: a weak band at shorter wavelength (320 nm in methylcyclohexane, MC) attributed to a vertical (Franck−Condon, FC) singlet state and a broad, stronger band at longer wavelength (475 nm in MC) that has been attributed either to an imidol tautomer or a twisted intramolecular charge-transfer (TICT) state or to the overlap of the tautomer and TICT fluorescence. Similar Stokes-shifted fluorescence is observed for *N*-methylbenzanilide (MBA), which is incapable of tautomer formation. An investigation of the room-temperature luminescence of BA, MBA, and several rigid derivatives by Azumaya et al.[4] led to the conclusions that (a) the weak short-wavelength emission is an artifact arising from an impurity and (b) the longer wavelength emission, which is absent in some rigid derivatives, arises from a TICT state, which is twisted about the amide C−N bond. Recent publications have reiterated assignments of the short-wavelength FC fluorescence and imidol tautomer fluorescence.[5,6]

The luminescence of BA in low-temperature glasses consists of a broad band attributed to overlapping fluorescence and phosphorescence. As initially noted by O'Connell et al.,[1] the fluorescence maximum occurs at longer wavelength than the phosphorescence maximum but at shorter wavelength than the room temperature fluorescence. We recently investigated the luminescence of a family of *N*-arylbenzamides both as microcrystalline solids and in methyltetrahydrofuran (MTHF) glasses at 77 K.[8] The fluorescence ($\lambda_{max} = 430$ nm) was assigned to a singlet state of undetermined configuration having a relaxed geometry and the phosphorescence to a planar π(aniline)−π^*-(delocalized) triplet state. The effects of phase and molecular structure on the luminescence behavior of BA and MBA suggested that this behavior is strongly dependent upon molecular conformation. To better define the relationships among molecular conformation, excited-state configuration, and luminescence, we have investigated the luminescence behavior of BA and MBA in MTHF over a wide range of temperatures and in the microcrystalline state at 77 and 298 K. The luminescence of two cyclic derivatives of MBA, *N*-phenylisoindole (PI) and the *N*-methyldibenzoazocinone (MDBA), in MTHF have also been investigated. The phenyl groups in PI and MDBA are constrained to E and Z configurations, analogous to those of the BA and MBA ground states (Scheme 1).[9] The experimental results are correlated with the ground- and excited-state potential energy surfaces, which have been constructed on the basis of RCIS calculations,[10] and with excited-state configurations obtained from ZINDO calculations.[11]

Experimental Section

General Methods. ^{1}H NMR spectra were measured on a Varian INOVA-500 MHz NMR spectrometer. UV−Vis spectra were measured on a Hewlett-Packard 8452A diode array spectrometer using a 1 cm path length quartz cell. Total emission spectra were measured on a SPEX Fluoromax spectrometer. Low-temperature spectra were measured either in a Suprasil quartz EPR tube (i.d. = 3.3 mm) using a quartz liquid nitrogen coldfinger dewar at 77 K or in an Oxford Cryogenics DN1704 cryostat fitted with an Oxford Instruments ITC4 temperature controller. Total emission quantum yields were measured by comparing the integrated area under the total emission curve at an equal absorbency and the same excitation wavelength as an external standard, 9,10-diphenyl anthracene ($\Phi_f \approx 1.0$ at 77K in MTHF).[12] The overlapping fluorescence and phosphorescence spectra were resolved by time-dependent integration as described previously.[8] All emission spectra are uncorrected, and the estimated error for the quantum yields is ±20%.

* To whom correspondence should be addressed. E-mail: lewis@chem.northwestern.edu.

† Part of the special issue "Noboru Mataga Festschrift".

10.1021/jp012013k CCC: $22.00
Published on Web 10/23/2001

SCHEME 1

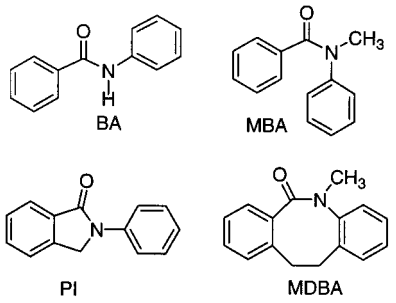

Fluorescence decays were measured on a Photon Technologies International (PTI) Timemaster stroboscopic detection instrument with a gated hydrogen or nitrogen lamp using a scatter solution to profile the instrument response function. Phosphorescence decays were measured on a PTI Timemaster phosphorescence-time-based detection instrument with a Xenon-flash lamp as the excitation source. Nonlinear least-squares fitting of the decay curves employed the Levenburg−Marquardt algorithm as described by James et al.[13] and implemented by the PTI Timemaster (version 1.2) software. Goodness of fit was determined by judging the χ^2 (<1.3 in all cases), the residuals, and the Durbin−Watson parameter (>1.6 in all cases). Solutions were degassed under vacuum (<0.1 Torr) through five freeze−pump−thaw cycles. Solid samples were measured in a Suprasil quartz EPR tube and similarly degassed without freezing.

All ab initio calculations were performed using Gaussian 98, revision A.7[10] on a 500 MHz Pentium III personal computer. The level of calculation is limited by the size of the molecules studied and the limit of computing power. The S1 state geometries were first optimized with RCIS method using a STO-3G basis set and then with a 3-21G basis set because direct optimization with a 3-21G basis set fails to converge. The T1-state geometries were optimized with the UHF method first using a STO-3G basis set and then using a 3-21G basis set. The S1 and T1 transition energies were calculated using the RCIS method.

ZINDO(S)/CI calculations were performed using Cache release 3.5 with ground-state structures optimized using the AM1 method using MOPAC (version 94.10) programs.[11] The 3D molecular structures were generated using Hyperchem version 5.0.

Materials. Benzanilide (BA) and *N*-methylbenzanilide (MBA) were puchased from Aldrich and recrystallized twice from DMF and acetone−hexane (1:1), respectively. Aniline, *o*-phthaldehyde, and 5,6,11,12-tetrahydrodibenz[*b*,*f*]azocine-6-one are comercially available and were used as received. Anhydrous MTHF containing 200 ppm BHT (Aldrich) was distilled over sodium under a nitrogen atmosphere.

4-N-Phenylisoindolinone (PI). The procedure of Grigg et al.[14] was modified. A mixture of *o*-phthaldehyde (2.7 g, 20 mmol) and aniline (1.9 mL, 20 mmol) in 20 mL of ethyl acetate and 5 mL of acetic acid was stirred under a nitrogen atomsphere at room temperature for 3 h. The resulting white precipitate was collected, washed with ether, and recrystallized with ethyl acetate and hexane (1:1) to give 1.9 g of PI (50%), mp 162−163 °C (lit.[14] 162−163 °C). ^{1}H NMR ($CDCl_3$, 500 MHz): δ 4.88 (s, 2H), 7.21 (t, ^3J = 7.0 Hz, 1H), 7.45 (t, ^3J = 8.0 Hz, 2H), 7.53 (t, ^3J = 7.5 Hz, 2H), 7.62 (t, ^3J = 7.0 Hz, 1H), 7.90 (d, ^3J = 8.0 Hz, 2H), 7.95 (d, ^3J = 7.5 Hz, 1H).

*N-Methyl-5,6,11,12-tetrahydrodibenz[b,f]azocine-6-one (MDBA).*A solution of NaH (0.24 g, 10 mmol) in 10 mL of DMF was added dropwise into a solution of 5,6,11,12-tetrahydrodibenz[*b*,*f*]azocine-6-one (1.1 g, 5 mmol) and MeI (0.63 mL, 10 mmol) in 20 mL of DMF. The resulting mixture was stirred for 2 h and then mixed with 50 mL water and extracted with 30 mL ethyl acetate. The organic layer was washed with brine and dried with anhydrous $MgSO_4$. After the solvent was removed on a rotavap, the residue was recrystallized from 1:1 ethyl acetate−hexane to give 0.7 g of MDBA (65%), mp 96−97 °C (lit.[15] 95−97 °C). ^{1}H NMR ($CDCl_3$, 500 MHz): δ 2.87−2.98 (m, 2H), 3.16−3.28 (m, 1H), 3.40 (s, 3H), 3.16−3.28 (m, 1H), 6.8−7.2 (m, 8H).

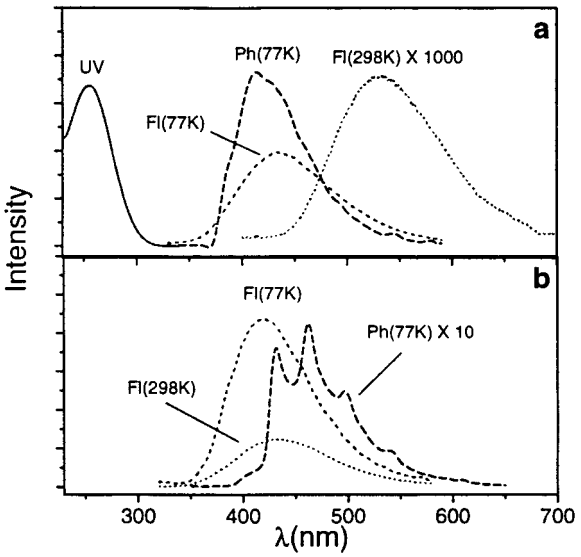

Figure 1. Absorption (solid line, λ = 262 nm, log ϵ = 4.16), fluorescence (short dash, 77 K; dotted, 298 K), and phosphorescence (dash, 77 K) spectra of benzanilide: (a) 0.1 mM in MTHF; (b) in microcrystals.

TABLE 1: Fluorescence Parameters for the Benzanilides[a]

		MTHF					solid	
	T, K	λ_{fl}, nm	τ_s, ns	Φ_{fl}	$10^{-8}\,k_{fl}$, s^{-1}	$10^{-8}\,k_{nr}$, s^{-1}	λ_{fl}, nm	τ_s, ns
BA	77	430	2.7	0.25	0.93	2.8	420	3.8
	298	520	0.4	0.0005	0.012	25	430	1.3
PI	77	400	4.6	0.60	1.3	0.9	405	4.1
	298	425	<0.1	0.007	1.4	200	405	1.8
MBA	77	500	2.7	0.01	0.037	3.6	460	5.1
	298	550	0.4	0.0002	0.005	25	480	2.3

[a] Structures shown in Scheme 1.

Results

Luminescence Spectra. The absorption and fluorescence spectra of BA in MTHF solution at 298 K are shown in Figure 1a. A single broad fluorescence band is observed with a maximum at 520 nm and a fluorescence quantum yield of 5×10^{-4}. The fluorescence decay is best fit by a single exponential with a decay time of 0.40 ns. Also shown in Figure 1a are the fluorescence and phosphorescence spectra of BA in a MTHF glass at 77 K. The overlapping spectra were resolved by time-dependent integration as previously described.[8] The luminescence spectra of microcrystalline BA obtained at 77 and 298 K are shown in Figure 1b. The fluorescence maxima at both temperatures are similar to that observed in the MTHF glass. The 77 K phosphorescence is strongly structured and its maximum occurs at longer wavelength than that in the glass. The luminescence parameters are summarized in Tables 1 and 2.

The temperature dependence of the fluorescence of BA in MTHF over the range of 77−343 K is shown in Figure 2.

TABLE 2: Phosphorescence Parameters for the Benzanilides[a]

		MTHF			solid	
	T, K	λ_{ph}, nm	τ_T	Φ_{ph}	λ_{ph}, nm	τ_T
BA	77	410	0.4 s	0.37	460	5.2 ms
PI	77	420	1.0 s	0.03	430	1.1 s
MBA	77	485	1.7 ms	0.02	450	4.1 ms
MDBA	77	398	0.9 s	0.01	430	4.0 ms

[a] Structures shown in Scheme 1.

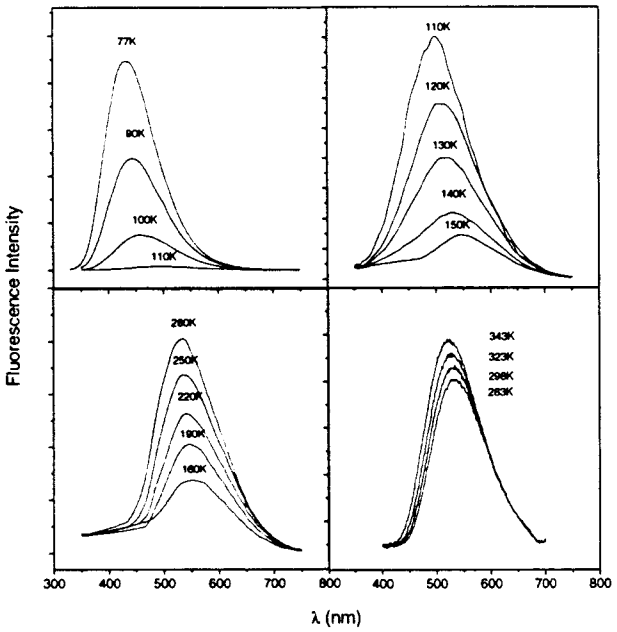

Figure 2. Fluorescence spectra of benzanilide (0.1 mM) in MTHF over the temperature range 77−343 K.

Between 77 and 150 K, the fluorescence intensity continuously decreases with increasing temperature and the emission maximum shifts from 430 to 550 nm. Above 150 K, the emission intensity increases as the maximum shifts to shorter wavelength reaching a value of 525 nm at 343 K. The temperature dependence of ν_{max} is shown in Figure 3. The phosphorescence intensity of BA also decreases with increasing temperature and is too weak to be observed when $T \geq 140$ K. The phosphorescence emission maximum shifts continuously from 416 nm at 77 K to 430 nm at 130 K (Figure 3).

The absorption and fluorescence spectra of PI in MTHF at 298 K are shown in Figure 4a along with its 77 K fluorescence and phosphorescence spectra. The fluorescence and phosphorescence spectra of microcrystalline PI are shown in Figure 4b. Emission maxima, quantum yields, and decay times are summarized in Tables 1 and 2. The fluorescence of PI undergoes only a small red shift on warming from 77 to 298 K in MTHF and no shift in the microcrystalline state. The emission maxima are at shorter wavelength than those of BA under all conditions. The fluorescence intensity of PI in MTHF decreases continuously with warming from 77 to 298 K; however, the total decrease in intensity is smaller than that observed for BA. The fluorescence maximum shifts to longer wavelength upon warming from 77 to 120 K but is essentially constant at higher temperatures (Figure 3).

The absorption and fluorescence spectra of MBA in MTHF at 298 K are shown in Figure 5a along with the 77 K fluorescence and phosphorescence spectra. The fluorescence and phosphorescence spectra of microcrystalline MBA are shown in Figure 5b. Emission maxima, quantum yields, and decay

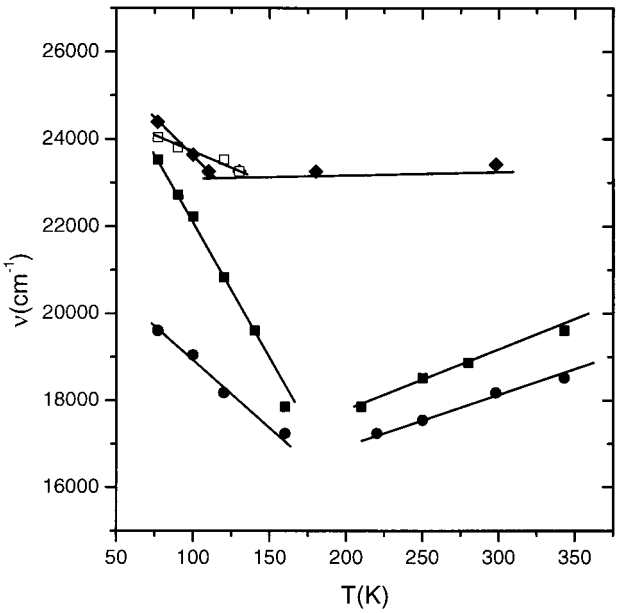

Figure 3. Plot of fluorescence maxima (ν, cm^{-1}) vs temperature (T, K) for BA (■), PI (◆), and MBA (●), and phosphorescence maximum of BA (□).

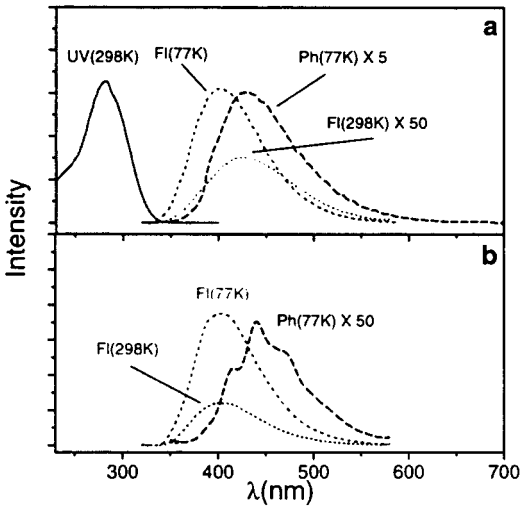

Figure 4. Absorption (solid line, $\lambda = 283$ nm, log $\epsilon = 4.25$), fluorescence (short dash, 77 K; dotted, 298 K), and phosphorescence (dash, 77 K) spectra of *N*-phenylisoindolinone: (a) 25 μM in MTHF; (b) in microcrystals.

times are summarized in Tables 1 and 2. Emission maxima are at longer wavelength for MBA than for BA, the difference being most pronounced at 77 K in MTHF, and the emission quantum yields are smaller for MBA than for BA. The temperature dependence of the fluorescence of MBA in MTHF (Figure 3) is qualitatively similar to that of BA. As is the case for BA, no phosphorescence is observed above 110 K.

The absorption spectrum of MDBA in MTHF at 298 K and its 77 K phosphorescence spectrum are shown in Figure 6. No fluorescence is observed at 77 or 298 K in either MTHF or the microcrystalline solid. The phosphorescence parameters are summarized in Table 2.

Calculated Ground- and Excited-State Energy Surfaces. The ground-state conformation of BA calculated by AM1 (gas phase) is fully planar (Figure 7a); the calculated amide and phenyl−amide dihedral angles are all <1°. Selected bond lengths and dihedral angles (Scheme 2) obtained from the AM1

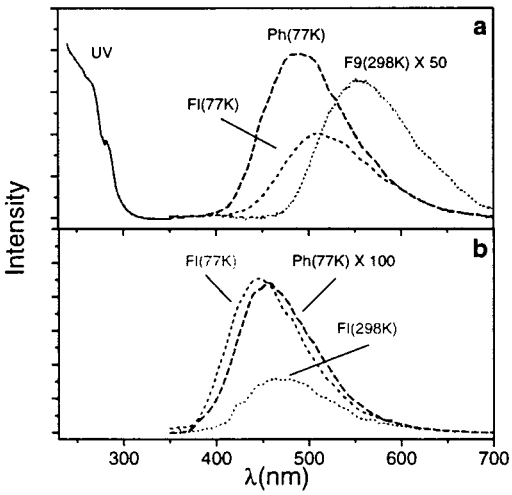

Figure 5. Absorption (solid line, $\lambda = 285$ (sh) nm, $\log \epsilon = 3.64$), fluorescence (short dash, 77 K; dotted, 298 K), and phosphorescence (dash, 77 K) spectra of *N*-methylbenzanilide: (a) 0.1 mM in MTHF; b) in microcrystals.

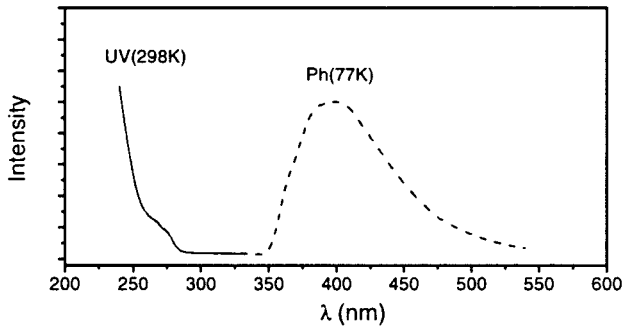

Figure 6. Absorption (solid line, $\lambda = 265$ nm (sh), $\log \epsilon = 3.11$) and phosphorescence (dash, 77 K) spectra of *N*-methyl-5,6,11,12-tetrahydrodibenz[*b*,*f*]azocine-6-one in MTHF (1 mM).

calculation are reported in Table 3 along with data for the crystal structure of BA, which displays a planar amide group with twisted phenyls. The barrier for 180° rotation about the amide C−N bond with optimization at each dihedral angle was calculated to be 6.5 kcal/mol with the Z isomer 1.3 kcal/mol higher in energy than the E isomer (Figure 8).

The ground-state conformations of PI, MBA, and MDBA calculated by AM1 are shown in Figure 7b−d, and their structural parameters are reported in Table 3. The calculated structure of PI, like that of BA, is fully planar (all dihedral angles <2°). The calculated structure of MBA possesses a small amide dihedral angle ($\theta_1 = 19°$ and $\theta_2 = 2°$) but large phenyl−amide angles ($\theta_3 = 44°$ and $\theta_4 = 66°$). The structure of MDBA, like that of MBA, is nonplanar, possessing moderate amide dihedral angles, ($\theta_1 = 16°$ and $\theta_2 = 7°$) and relatively large phenyl−amide dihedral angles ($\theta_3 = 62°$ and $\theta_4 = 50°$). Ground-state geometries have also been optimized using Gaussian at the 3-21G level. The results (not shown) are similar to those obtained using AM1.

The optimized geometries of the lowest energy singlet states of all four amides are reported in Table 3 and shown in Figure 7a−d. The geometries were first optimized with the RCIS method using a STO-3G basis set and then with a 3-21G basis set (except in the case of MDBA). This two-step procedure was necessary to obtain convergence for the 3-21G calculations. The S_1 geometries are notable in several respects. In the case of BA and MBA, the amide group becomes nearly orthogonal (θ_1 and $\theta_2 \approx 77°-100°$) while the benzoyl and aniline groups

SCHEME 2

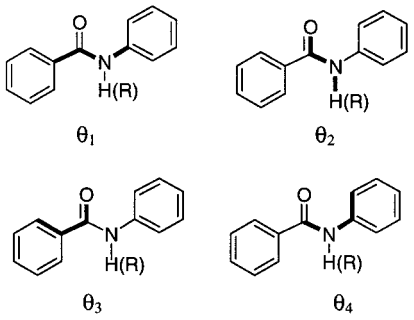

TABLE 3: Geometric Parameters for Benzanilide Ground and Excited Singlet States[a]

	dihedral angles[b]				bond lengths, Å			
	θ_1°	θ_2°	θ_3°	θ_4°	CO−N	Ph−CO	Ph−N	C−O
BA, S_0[c] crystal	180	180	31	32	1.35	1.48	1.41	1.28
BA, S_0 calcd	180	180	0	0	1.39	1.50	1.41	1.25
BA, S_1 relaxed	(180)	119	0.3	7	1.42	1.47	1.40	1.32
BA, S_1 opt	95	77	0.7	2	1.41	1.44	1.40	1.30
PI, S_0 calcd	180	180	0	0	1.42	1.49	1.40	1.24
PI, S_1 opt	168	150	30	13	1.42	1.46	1.39	1.31
MBA, S_0[c] crystal	14		48	60	1.36			
MBA, S_0 calcd	19	2	44	65	1.40	1.49	1.42	1.25
MBA, S_1 opt	101	79.0	2	6	1.41	1.43	1.41	1.30
MDBA, S_0 calcd	16	7	62	59	1.40	1.49	1.42	1.25
MDBA, S_1 opt	62	44	3	51	1.462	1.48	1.47	1.32

[a] Structures shown in Scheme 1. [b] Dihedral angles defined in Scheme 2. [c] Crystal data from ref 9a.

remain planar (θ_3 and $\theta_4 \leq 7°$). Less pronounced changes are obtained for PI, values of $\Delta\theta \leq 30°$ being observed for all of the dihedral angles. Intermediate amide dihedral angles are obtained for S_1 in MDBA ($\theta_1 = 62°$ and $\theta_2 = 43°$), along with a small phenyl−carbonyl dihedral angle ($\theta_3 = 3°$) and large phenyl−nitrogen dihedral angle ($\theta_4 = 51°$). For all four of the amides, the calculated amide C═O bond length increases and the Ph−CO bond length decreases for S_1 vs S_0. Changes in the other bond lengths are dependent upon structure.

The singlet and triplet excited-state structures and energies for BA have also been calculated for several restricted geometries, including the calculated ground-state geometry (flat) and several geometries in which the amide dihedral angle (θ_1) is fixed and all other structural parameters are minimized. The results are shown in Figure 8. Starting with the planar ground-state geometry (GS), the excited state geometry is allowed to relax while retaining a totally planar structure (flat), and then by fixing $\theta_1 = 180°$ but optimizing all other geometric parameters (180). These small-amplitude geometric changes decrease the S_1 energy but increase the S_0, S_2, and T_1 energies. The minimized geometry for S_1 with a fixed angle of $\theta_1 = 180°$ is reported in Table 3 along with values for the other dihedral angles and bond lengths, which are similar to those for the fully optimized structure.

With the optimized $\theta_1 = 180°$ S_1 structure used as a starting point, the value of θ_1 is incrementally decreased to 10°, similar to the ground-state value for MBA (Table 3). The results are shown in Figure 8. The energy of the vibrationally excited ground-state S_0^* is considerably higher than that of the optimized ground-state S_0 and changes only slightly with decreasing θ_1. The energy of S_1 decreases as θ_1 increases, reaching a minimum value for $\theta_1 = 95°$. The energy of T_1 calculated using the S_1-minimized geometries is independent of the value of θ_1. The dependence of the T_1 energy on θ_1 has also been calculated

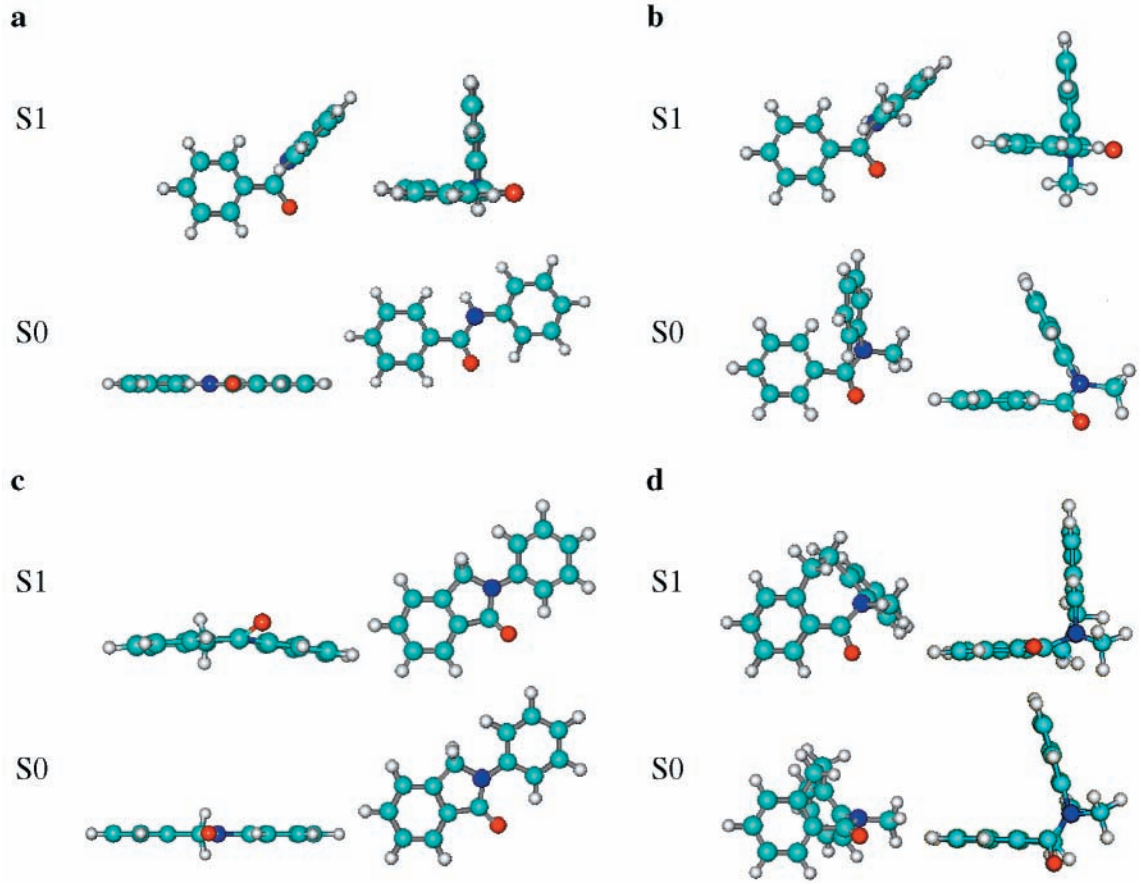

Figure 7. Optimized singlet ground-state and lowest excited-state geometry for BA (a), MBA (b), PI (c), and MDBA (d).

using the UHF method and displays a shallow minimum for a twisted geometry (Figure 8).

The calculated $S_0 \rightarrow S_1$ transition energies of BA for the ground-state, partially optimized ($\theta_1 = 180°$), and fully optimized S_1 structures are reported in Table 4. The energies are seen to decrease with increasing structural relaxation. The transition energies of the fully optimized S_1 structures for PI and MBA are also reported in Table 4 along with the observed values of the fluorescence maxima in the nonpolar solvent methylcyclohexane (MC). The calculated values correspond to 0,0 transitions and thus are at higher energy than the values of λ_{fl}. Scaling the calculated energies by a factor of 1.5 provides values that are in better agreement with the values of λ_{fl}.

ZINDO Calculations. We have previously employed semiemperical INDO/S SCF-CI calculations using the algorithm developed by Zerner and co-workers[11] to investigate the electronic structure of the vertical (FC) excited singlet and triplet states of BA. The results are summarized in Table 5 along with the results of ZINDO calculations for the singlet and triplet states of BA possessing the optimized S_1 geometry. Twisting about the amide bond is seen to result in a large decrease in S_1, S_2, and T_1 energies but only a small decrease in the S_3 energy. All of the twisted states have low oscillator strengths. Twisting is seen to result in mixing of the character of the FC S_1 and S_3 states producing twisted singlet states with mixed n,B* and A,B* character (see Table 5, footnote d). The character of the lowest triplet changes from A,AB* to A,B* upon twisting. The ZINDO calculated S_1 energies for the optimized geometries of BA, PI, and MBA are reported in Table 4 and are seen to be in reasonable agreement with the scaled values obtained from RCIS calculations.

Discussion

Benzanilide Fluorescence. We previously reported that the fluorescence of BA at room temperature in MC solution consists of a single broad band with a large Stokes shift ($\lambda_{max} = 475$ nm).[7] An even larger Stokes shift is observed for the fluorescence in MTHF solution (Figure 1a, $\lambda_{max} = 520$ nm). The fluorescence decay time is shorter in MTHF (0.40 ns) than in MC solution (0.86 ns). No fluorescence is observed at room temperature in more polar nitrile or alcohol solvents. The fluorescence decay of BA in both MC and MTHF solutions is best fit by a single exponential (Table 2). Azumaya et al.[4] assigned the room-temperature fluorescence of BA to a single excited state of TICT character on the basis of the absence of Stokes-shifted fluorescence from analogues of BA that are unable to undergo large-amplitude twisting about the amide C−N bond. Our results are in agreement with this assignment.

BA displays strong fluorescence and phosphorescence at 77 K in MTHF with maxima at 430 and 416 nm, respectively. Similar emission maxima were observed by O'Connell et al.[1] in the more polar EPA glass. We have attributed the higher energy of the fluorescence maximum in the glass vs solution to the rigid nature of the glass, which prevents the large amplitude geometric change necessary for formation of the relaxed TICT state.[8] The fluorescence maximum in microcrystalline BA at both 77 and 298 K is similar to that in MTHF at 77 K (Table 1), in accord with the dependence of the Stokes shift upon large amplitude geometry change.

To establish the connection between the room temperature and 77 K luminescence of BA, a detailed investigation of the temperature dependence was undertaken. MTHF was the solvent of choice for these studies because it forms glasses with good

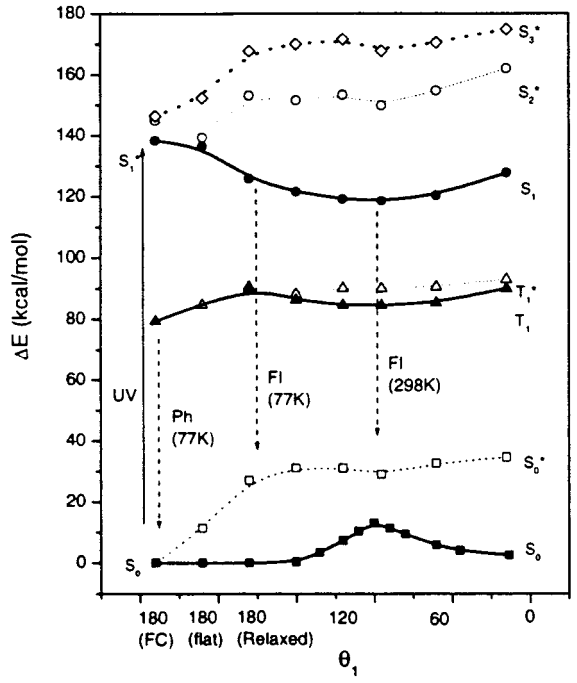

Figure 8. Calculated potential energy curves for benzanilide obtained at various geometries. FC is the optimized planar ground-state geometry. The S_1 geometry is kept planar, but bond angles and bond lengths are allowed to relax in flat. The amide dihedral angle θ_1 is fixed at 180°, but all other bond lengths and bond angles are allowed to relax in relaxed. With relaxed used as the starting point, the amide dihedral angle θ_1 is incrementally decreased from 180° to 20°. Solid lines are optimized S_0 (■, AM1), S_1 (●, RCIS/3-21G), and T_1 (▲, UHF/3-21G) states. Dashed lines are the hot ground-state S_0^* (□), S_2^* (○), S_3^* (◇), and T_1^* (△) states obtained from calculations using optimized S_1 geometries. Vertical arrows correspond to proposed geometries for phosphorescence at 77 K and fluorescence at 77 and 298 K.

optical properties and its physical properties are well-characterized over a broad temperature range.[16,17] Moreover, all of the amides remain soluble at low temperatures, thus avoiding problems with amide aggregations, which have been reported to occur in nonpolar glasses including MC.[6] Warming the glass from 77 to 160 K results in a continuous decrease in fluorescence intensity and a red shift in the emission maximum (Figures 2 and 3). On further warming a continuous blue shift and increase in intensity are observed. The thermochromic shifts[18] obtained from the slopes of Figure 3 are summarized in Table 6.

Two properties of the MTHF glass, its viscosity and dielectric constant, are expected to affect the fluorescence maximum and intensity. The viscosity of the glass decreases exponentially with increasing temperature from 3.7×10^{20} P at 77 K to 2.1×10^3 P at 107.5 K, slightly below the glass-transition temperature ($T_g \approx 120$ K).[16] Nonexponential dependence of the viscosity upon temperature is expected at higher temperatures. Below T_g, the dielectric constant of MTHF has a constant value of $\epsilon = 2.6$[17], and thus, the shift in emission maximum should be determined mainly by the solvent viscosity. A plot of ν_{fl} vs T at low temperatures (Figure 3) has a slope of -63 cm^{-1}/K. Decreased viscosity should facilitate geometric relaxation of the Franck−Condon excited state to the relaxed state, which emits at longer wavelength.

Upon melting, the MTHF dielectric constant increases rapidly to a maximum value of $\epsilon \approx 18$ at 140 K and then continuously decreases to a value of 7.0 at 298 K.[17] The high solvent polarity around 150 K should stabilize the geometrically relaxed TICT state, thus accounting for the large red shift in λ_{fl} at this

TABLE 4: Calculated and Observed S_1 State Transition Energies for the Benzanilides[a]

	ΔE, kcal[b]	λ_{calcd}, nm[b]	λ_{scaled}, nm[c]	λ_{ZINDO}, nm[d]	λ, nm[e]
BA, FC	132	217	326		
BA, relaxed	99	290	434		430[f]
BA, opt	90	320	479	473	475[g]
PI, opt	106	269	403	416	422[g]
MBA, opt	89	322	483	460	515[g]

[a] Structures shown in Scheme 1. [b] Singlet energy calculated using Gaussian (RCIS method). [c] Scaling factor of 1.5. [d] Singlet energy calculated using ZINDO. [e] Experimental values. [f] Data for MC at 77 K from ref 7. [g] Room-temperature data from ref 4.

TABLE 5: ZINDO-Calculated Energy, Wavelength, Oscillator Strength, and Character of the Benzanilide Excited States

BA state[a]	ΔE, kcal[b]	λ_{calcd}, nm[b]	f[c]	character[d]
S_1, FC	79.9	358	0.0002	n,B*
S_1, opt	60.4	473	0.0002	n,B*; A,B* [e]
S_2, FC	102.1	280	0.08	A,A*
S_2, opt	86.0	332	0.0005	n,B*; A,B* [f]
S_3, FC	103.6	276	0.37	A,B*
S_3, opt	101.4	282	0.033	A,A*
T_1, FC	68.1	420		A,AB*
T_1, opt	45.0	634		A,B*

[a] FC = vertical (Franck−Condon), opt = optimized S_1 geometry. [b] ZINDO-calculated energy and wavelength. [c] Oscillator strength. [d] Character of the excited state, n = nonbonding (CO), A = aniline localized, B = π benzoyl localized, AB = π delocalized. [e] 37% n,B*, 51% A,B*. [f] 46% n,B*, 46% A,B*.

TABLE 6: Thermochromic Shifts[a]

	low-temp shift,[b] cm^{-1}/K	high-temp shift,[c] cm^{-1}/K
BA, S_1	−63	13
BA, T_1	−12	
PI	−34	1
MBA	−29	11

[a] Structures shown in Scheme 1. [b] Slope of Figure 3, $T < 150$ K. [c] Slope of Figure 3, $T > 150$ K.

temperature. The increase in fluorescence intensity at higher temperatures is consistent with the stronger fluorescence observed in nonpolar vs polar solvents at room temperature. A plot of ν_{fl} vs T at high temperatures (Figure 3) has a slope of 13 cm^{-1}/K. The thermochromic shift for BA in MTHF (Table 6) is smaller than the value of 21 cm^{-1}/K reported for 4-dimethylaminobenzonitrile (DMABN).[18] The excited-state dipole moment for BA can be calculated from the thermochromic shift, the ground-state dipole moment ($\mu_g = 5.1$ D), and the estimated molecular radius ($r = 4.5$ Å) using the method of Hagen et al.[18] The resulting value of $\mu_e = 15$ D is somewhat smaller than the value of $\mu_e = 19.5$ D obtained by this method for the TICT state of DMABN.[18] Thus, the relaxed singlet state of BA can be characterized as possessing substantial ICT character.

The phosphorescence behavior of BA in MTHF is also temperature-dependent. The maximum displays a modest red shift upon warming from 77 to 130 K, a plot of ν_{ph} vs T having a slope of 12 cm^{-1}/K (Figure 3). This slope is much smaller than that observed for the low-temperature fluorescence of BA, suggesting that geometric relaxation is less extensive for the triplet vs singlet state. No phosphorescence is observed at temperatures greater than 130 K, plausibly because of diffusive quenching of the long-lived triplet state by traces of oxygen or other quenching impurities.

Benzanilide Potential Energy Surfaces. The low-temperature viscosity dependence of BA luminescence suggests that its fluorescence behavior is dependent upon the extent of excited-state geometric relaxation. The calculated optimized geometries of BA in the ground and lowest excited singlet states are shown in Figure 7a, and the amide dihedral angles (Scheme 2) and bond lengths are reported in Table 3. The calculated (gas phase) ground state is planar. In the crystal structure, BA molecules are assembled into a one-dimensional hydrogen-bonded tape in which both phenyl groups are twisted by ca. 30° from the amide plane.[9] Crystal packing forces evidently are sufficiently large to overcome the small barriers for twisting about the phenyl−amide bonds. In solution, BA exists exclusively (>99%) as the E isomer (Scheme 1). The calculated (AM1) barrier for S_0 (ground state) amide rotation is 6.5 kcal/mol, and the E isomer is more stable than the Z isomer by 1.3 kcal/mol (Figure 8). This barrier is lower than that obtained previously using MM2 calculations without optimization (16 kcal/mol)[7] or the barrier estimated for MBA from NMR coalescence temperature for the E and Z isomers (13.3 kcal/mol).[9]

The optimized S_1 geometry has large amide dihedral angles but small phenyl−amide dihedral angles (Table 3). Thus, the planar benzoyl and anilide groups are approximately perpendicular (Figure 7a). These changes are accompanied by a decrease in the Ph−CO bond length and increases in the amide C═O and C−N bond lengths. Twisting about the amide C−N bond is the dominant large amplitude geometry change that occurs upon relaxation of the planar Franck−Condon (FC) singlet state to the optimized S_1 geometry. The energy of the FC excited-state S_1 is found to decrease and the S_0 energy to increase as the planar geometry is allowed to relax in stages, first by retaining a planar geometry but optimizing bond lengths and angles (flat geometry) and then by retaining a dihedral angle of $\theta_1 = 180°$ but removing all other geometric constraints (180° relaxed geometry, Figure 8). Such small-amplitude geometry changes plausibly can occur in the highly viscous MTHF glass and the microcrystalline state and can account for the Stokes-shifted fluorescence observed in these media (Figure 1).

Next, with the relaxed 180° geometry used as the starting point, the effect of large-amplitude amide torsion was investigated. The S_1 energies decrease with increasing geometric relaxation, reaching a minimum value for $\theta_1 = 95°$ (Figure 8, bold line). The S_0 energies calculated using the S_1-minimized geometries show little variation with θ_1 (Figure 8, dashed line). These S_0 energies correspond to vibrationally excited ground-state geometries and thus lie at higher energies than the AM1-minimized ground state. The calculated S_1-S_0 energy gaps and corresponding wavelengths for the FC, 180° relaxed, and fully relaxed geometries of BA are reported in Table 3. Even for the fully relaxed geometry, the calculated wavelength is considerably shorter than the observed emission maxima in rigid media (Table 4). Application of a scaling factor of 1.5 to the calculated singlet energies, provides scaled energies that correspond to fluorescence maxima at 434 and 479 nm for the relaxed 180° geometry and fully relaxed excited states, respectively. These values are in good agreement with the emission maxima in rigid media and in fluid solution. The singlet energy calculated for the optimized singlet-state geometry using ZINDO (447 nm) is similar to the scaled value. The appearance of the S_1 potential energy surface in Figure 8 indicates that there is no barrier for large-amplitude twisting about the amide bond. The temperature dependence of the fluorescence intensity and maxima below 150 K are consistent with the presence of a small, viscosity-imposed barrier for large-amplitude amide twisting.

The calculated T_1 potential energy surface differs from the S_1 surface in that the planar FC geometry is an energy minimum. This is consistent with the relatively small thermochromic shift observed for the phosphorescence maximum upon warming the MTHF glass from 77 to 130 K (Figure 3).

The effect of molecular geometry upon the luminescence behavior of BA can be summarized with reference to Figure 8. Electronic excitation populates the planar FC singlet state, which can undergo intersystem crossing to yield the planar triplet state, which emits with $\lambda_{ph} = 416$ nm. In rigid media (MTHF glass or microcrystals), the FC singlet state undergoes small-amplitude geometric relaxation effecting a decrease in the S_1 energy and an increase in the S_0 energy. This results in emission with $\lambda_{fl} = 430$ nm, a slightly longer wavelength than λ_{ph} (Figure 1). In fluid solution, the lowest singlet state can undergo large-amplitude geometric relaxation, resulting in a further red shift in the fluorescence maximum to $\lambda_{fl} = 520$ nm.

Excited-State Electronic Configuration and Dynamics. We previously reported the results of ZINDO calculations for the planar Franck−Condon singlet and triplet states of BA (Table 5). According to these calculations, the planar S_1 state has benzoyl-localized n,π* character (n,B*) similar to that of acetophenone. The absence of fluorescence from the FC singlet state is consistent with this assignment. The nearly-degenerate S_2 and S_3 states have π,π* character, S_2 being localized on aniline (A,A*) and S_3 being delocalized (A,B*). The character of the π,π* T_1 state is similar to that of S_3. The relatively long triplet lifetime (Table 2) and structured phosphorescence observed in microcrystalline BA (Figure 1b) are consistent with this assignment.

The two lowest energy excited singlet states with optimized twisted geometry are predicted to have extensive configuration interaction dominated by the n,B* and A,B* configurations. The calculated singlet-state potential energy surfaces (Figure 8) indicate the presence of an avoided crossing between the two lowest singlet states that occurs upon low-amplitude geometric relaxation. The relatively short singlet lifetime ($\tau_s = 2.7$ ns) and occurrence of intersystem crossing at 77 K ($\Phi_{isc} \geq \Phi_{ph} = 0.37$) are consistent with the mixed n,π* and π,π* character of the partially relaxed singlet state. On the assumption that nonradiative decay at 77 K is dominated by intersystem crossing, a value of $k_{isc} = 2.8 \times 10^8\ s^{-1}$ can be estimated for BA (Table 1). This value is distinctly smaller than that for the n,π* state of acetophenone ($4 \times 10^{11}\ s^{-1}$) but larger than that for the π,π* state of 1-phenylpropene ($5 \times 10^7\ s^{-1}$).[19,20]

Solvation of the fully twisted singlet presumably enhances the TICT character of the twisted singlet state in fluid solution. This change is accompanied by a large decrease in the fluorescence rate constant and increase in the nonradiative rate constant (Table 1). These changes result in a much larger decrease in Φ_{fl} than in τ_s at 298 vs 77 K.

Fluorescence of PI, a Planar E Analogue. According to the AM1 calculations, PI is planar in the ground state with the two phenyl groups fixed in the E configuration (Figure 7b). Twisting about the amide bond is restricted by the lactam ring. Azumaya et al.[4] observed that the fluorescence maximum for PI in MC solution occurs at 422 nm, considerably blue-shifted with respect to the emission of BA (477 nm in MC). In addition, unlike BA, which is nonfluorescent in ethanol solution, more intense emission with a maximum of 442 nm is observed for PI in ethanol vs MC solution.[4] The behavior of PI was attributed to its rigid structure, which precludes extensive twisting about the amide C−N bond. We observe a fluorescence maximum at

425 nm for PI in MTHF at 298 K (Figure 4), intermediate between the values for MC and for ethanol solution.

O'Connell et al.[1] observed fluorescence from PI in the polar mixed solvent EPA both at room temperature and in a rigid glass at 77 K. Upon warming from 77 K to room temperature, the emission maximum shifts from 410 to 450 nm and the intensity decreases ca. 50-fold. We observe emission maxima at 400 nm for PI in a MTHF glass and at 405 nm in microcrystalline PI both at 77 and 298 K (Figure 4, Table 1). Upon warming the glass from 77 to 100 K, there is a decrease in the fluorescence intensity and a red shift in the maximum from 400 to 430 nm (Figure 3) attributed to small-amplitude geometric relaxation. The thermochromic shift for PI (Table 6) is approximately half that of BA. Above T_g, the emission intensity continues to decrease with increasing temperature, but unlike BA, there is little further red shift. The absence of thermochromism at higher temperature indicates that the singlet state of PI is relatively nonpolar, in accord with its inability to form a TICT state.

According to the RCIS-minimized calculations, the PI singlet state is less planar than the ground state (Figure 7b). Deformation of the lactam ring is pronounced, with changes in both amide dihedral angles, θ_1 and θ_2, and in the phenyl−CO dihedral angle, θ_3 (Table 2). However, the phenyl−amide dihedral angle, θ_4, remains small. Thus, we assign the small red shift observed upon warming of the MTHF glass to geometric relaxation of the lactam ring. The scaled value of the PI S_0-S_1 energy gap calculated using the minimized S_1 geometry corresponds to 403 nm, and the value obtained from a ZINDO calculation is 416 nm, both slightly shorter wavelengths than the 422 nm emission maximum in MC solution.

The singlet lifetime of PI at 77 K is somewhat longer than that of BA, as a consequence of its slower nonradiative rate constant (Table 1). The fluorescence rate constant for PI is similar to that for BA, resulting in a larger value of Φ_{fl} for PI. At 298 K, the singlet lifetime of PI is too short to measure with our lifetime apparatus (<0.1 ns). Azumaya et al.[4] report a lifetime of less than 30 ps in MC solution.

Fluorescence of MBA and MDBA, Nonplanar Z Analogues. The AM1-calculated ground-state structure of MBA is highly nonplanar (Figure 7c) and is similar to its crystal structure (Table 3).[9a] Both the calculated and observed amide dihedral angles are small ($\theta_1 = 15°$ and $\theta_2 = 2°$), whereas both phenyl−amide dihedral angles are large ($\theta_3 = 45°$ and $\theta_4 = 62°$). This is consistent with larger amide vs benzoyl or aniline resonance energies. The calculated ground-state structure of MDBA (Figure 7d) is similar to that of MBA, with small amide dihedral angles ($\theta_1 = 16°$ and $\theta_2 = 7°$) and large phenyl−amide dihedral angles ($\theta_3 = 62°$ and $\theta_4 = 60°$).

Very weak Stokes-shifted fluorescence is observed for MBA in fluid solution with fluorescence maxima of 518 nm in MC and 550 nm in MTHF. This emission was attributed by Azumaya et al.[4] to a TICT state. No fluorescence is observed for MBA at 298 K in polar solvents. MDBA is nonfluorescent in both nonpolar and polar solvents.

The fluorescence maximum of MBA in MTHF at 77 K is at 500 nm, similar to the value observed by Heldt et al.[6] for MC solution. The fluorescence maxima in microcrystalline MBA at both 77 and 298 K are at shorter wavelengths, 460 and 480 nm, respectively (Table 1). Upon warming the MTHF glass from 77 to 343 K, changes in fluorescence maxima and intensities similar to those for BA are observed (Figure 3). The low-temperature thermochromic shift is considerably smaller than that for BA (Table 6), indicative of a smaller difference between the relaxed and FC S_1 geometries. The high-temperature shift is similar to that for BA, indicative of TICT states with similar dipole moments for MBA and BA. No fluorescence is observed for MDBA in MTHF at 77 K or in the microcrystalline solid.

The minimized geometry of the lowest singlet state of MBA is shown in Figure 7c. As is the case for BA, the amide group is twisted in the singlet state ($\theta_1 = 101°$ and $\theta_2 = 79°$) and the benzoyl and aniline groups are more nearly planar than in the ground state ($\theta_3 = 2°$ and $\theta_4 = 6°$). Thus, large amplitude motions are necessary to convert the FC excited state to the relaxed singlet. The smaller Stokes shift observed at 77 K in crystalline MBA than in MTHF glass may reflect the greater rigidity of the former environment. Assuming that the S_1 potential energy surface for MBA resembles that for BA (Figure 8), there should be no barrier other than that imposed by the medium for amide rotation from the FC state ($\theta_1 = 19°$) to the fully optimized S_1 geometry ($\theta_1 = 101°$).

The minimized geometry of the singlet state of MDBA is shown in Figure 7d. The amide dihedral angles are smaller than those for MBA ($\theta_1 = 62°$ and $\theta_2 = 43°$), presumably due to restricted torsion in the dibenzazocineone ring system.[15] The benzoyl group dihedral angle is small ($\theta_3 = 3.0°$), as is the case for the other benzanilides; however, the phenyl−nitrogen dihedral angle is much larger ($\theta_4 = 51°$) than for the other benzanilides.

The singlet decay time for MBA at 77 K is similar to that of BA in both MTHF and the crystalline state. However, both the fluorescence quantum yield and rate constant are considerably smaller for MBA. This may reflect the fact that the less-planar MBA has smaller Franck−Condon factors for radiative decay. Nonradiative decay rates are similar for BA and MBA at both 77 and 298 K. Our failure to detect fluorescence from the nonplanar MDBA could reflect a low value of k_{fl}.

All of the benzamides display phosphorescence at 77 K both in MTHF glasses and in microcrystalline solids. Phosphorescence in MTHF is structureless, whereas the phosphorescence of crystalline BA and PI is structured. The E amides, BA and PI, which are expected to have planar triplet states, have similar values of λ_{ph} and τ_T in MTHF glasses (Table 2). The longer wavelength emission of MBA may reflect either differences in geometry or the effect of *N*-methylation on the frontier orbital energies. The higher energy of the MDBA phosphorescence is somewhat surprising in view of the similarity of its ground-state structure to that of MBA (Table 3). The more rigid structure of MDBA may break the conjugation between the benzoyl and aniline groups. The value of λ_{ph} for MDBA is, in fact, similar to that for benzamide at 77 K in a MTHF glass. Like MDBA, benzamide is nonfluorescent at both 77 and 298 K in MTHF.

Concluding Remarks. The combination of experimental investigation of the temperature-dependent luminescence of BA and several analogues with computational studies of the ground- and excited-state potential energy surfaces and electronic configuration has permitted further elucidation of the complex excited-state behavior of these molecules. Studies of the temperature dependence of BA luminescence over the entire 77−298 K temperature range serve to connect the results of previous studies obtained at a single temperature. The thermochromic behavior of BA displays two distinct temperature regimes: a low-temperature regime in which decreasing viscosity of the MTHF glass permits increased geometric relaxation, resulting in a red shift and decreased fluorescence intensity and a high-temperature regime in which decreasing solvent polarity results in a blue shift and increased fluorescence intensity. An excited-state dipole moment of 15 D is estimated from the high-

temperature thermochromism data. In contrast, BA phosphorescence shows only modest thermochromic shifts at low temperatures, and no phosphorescence is observed in fluid solution.

These results can be understood using the calculated ground- and excited-state potential energy surfaces and excited-state configurations. The geometry of the π,π^* triplet state is similar to that of the ground state, and thus, its emission maximum changes only slightly as the MTHF glass is warmed from 77 K. In contrast, the Franck−Condon n,π^* singlet state undergoes small-amplitude geometric changes even in the 77 K glass or crystalline solid. The resulting decrease in S_1-S_0 energy gap shifts the fluorescence maximum to longer wavelength than the phosphorescence maximum. Above the solvent glass transition temperature, the S_1 state can undergo large-amplitude twisting about the amide C−N bond resulting in the formation of a TICT state that is responsible for the weak Stokes-shifted fluorescence observed in fluid solution. The luminescence behavior of PI, MBA, and MDBA can also be correlated with their ground- and excited-state geometries. Small-amplitude singlet-state geometric relaxation occurs even for the cyclic analogue PI.

The potential energy surfaces for BA bear some similarity to the well-characterized surfaces for the stilbenes[21] in that twisting about the central C−N or C═C bond results in a maximum on the ground state and shallow minima in the excited singlet and triplet surfaces. There are, however, several significant differences in the behavior of the benzamides and stilbenes.[21] First, the relaxed BA singlet undergoes intersystem crossing at 77 K, whereas the stilbene singlet does not. This difference plausibly reflects the n,π^* character of the relaxed BA singlet. Second, there is a small barrier for twisting of singlet stilbene but not for twisting of BA, resulting in the observation of fluorescence from the FC state of stilbene but not from BA. Third, the twisted singlet of stilbene is nonfluorescent as a consequence of its very short singlet lifetime, whereas twisted BA is weakly fluorescent and has a moderately long singlet lifetime. This difference may reflect the higher S_0 energy for twisted stilbene, which results in a smaller S_0-S_1 energy gap. Presumably, BA, like stilbene, undergoes efficient E,Z photoisomerization. However, the low barrier for BA thermal isomerization (Figure 8) would require the use of low-temperature methods to detect the Z isomer of BA or the E isomer of MBA.

Acknowledgment. Funding for this project was provided by NSF Grants CHE-9734941 and CHE-0100596.

References and Notes

(1) O'Connell, E. J., Jr.; Delmauro, M.; Irwin, J. *J. Photochem. Photobiol.* **1971**, *14*, 189.

(2) Tang, G.-Q.; MacInnis, J.; Kasha, M. *J. Am. Chem. Soc.* **1987**, *109*, 2531−2533.

(3) Heldt, J.; Gormin, D.; Kasha, M. *J. Am. Chem. Soc.* **1988**, *110*, 8255−8256.

(4) Azumaya, I.; Kagechika, H.; Fujiwara, Y.; Itoh, A.; Yamaguchi, K.; Shudo, K. *J. Am. Chem. Soc.* **1991**, *113*, 2833−2838.

(5) Lucht, S.; Stumpe, J.; Rutloh, M. *J. Fluoresc.* **1998**, *8*, 153−166.

(6) Heldt, J.; Heldt, J. R.; Szatan, E. *J. Photochem. Photobiol., A* **1999**, *121*, 91−97.

(7) Lewis, F. D.; Long, T. M. *J. Phys. Chem. A* **1999**, *102*, 5327.

(8) Lewis, F. D.; Liu, W.-Z. *J. Phys. Chem. A* **1999**, *103*, 9678.

(9) (a) Itai, A.; Toriumi, Y.; Tomioka, N.; Kagechika, H.; Azumaya, I.; Shudo, K. *Tetrahedron Lett.* **1989**, *30*, 6177. (b) Azumaya, I.; Yamaguchi, K.; Kagechika, H.; Saito, S.; Itai, A.; Shudo, K. *Yakugaku Zasshi* **1994**, *114*, 414. (c) Azumaya, I.; Kagechika, H.; Yamaguchi, K.; Shudo, K. *Tetrahedron* **1995**, *51*, 5277.

(10) Frisch, M. J.; Trucks, G. W.; Schlegel, H. B.; Scuseria, G. E.; Robb, M. A.; Cheeseman, J. R.; Zakrzewski, V. G.; Montgomery, J. A., Jr.; Stratmann, R. E.; Burant, J. C.; Dapprich, S.; Millam, J. M.; Daniels, A. D.; Kudin, K. N.; Strain, M. C.; Farkas, O.; Tomasi, J.; Barone, V.; Cossi, M.; Cammi, R.; Mennucci, B.; Pomelli, C.; Adamo, C.; Clifford, S.; Ochterski, J.; Petersson, G. A.; Ayala, P. Y.; Cui, Q.; Morokuma, K.; Malick, D. K.; Rabuck, A. D.; Raghavachari, K.; Foresman, J. B.; Cioslowski, J.; Ortiz, J. V.; Stefanov, B. B.; Liu, G.; Liashenko, A.; Piskorz, P.; Komaromi, I.; Gomperts, R.; Martin, R. L.; Fox, D. J.; Keith, T.; Al-Laham, M. A.; Peng, C. Y.; Nanayakkara, A.; Gonzalez, C.; Challacombe, M.; Gill, P. M. W.; Johnson, B. G.; Chen, W.; Wong, M. W.; Andres, J. L.; Head-Gordon, M.; Replogle, E. S.; Pople, J. A. *Gaussian 98*, revision A.7; Gaussian, Inc.: Pittsburgh, PA, 1998.

(11) Zerner, M. C.; Loew, G. H.; Kirchner, R. F.; Mueller-Westerhoff, U. T. *J. Am. Chem. Soc.* **1980**, *102*, 589.

(12) Li, R.; Lim, E. C. *J. Chem. Phys.* **1972**, *57*, 605.

(13) James, D. R.; Siemiarczuk, A.; Ware, W. R. *Rev. Sci. Instrum.* **1992**, *63*, 1710.

(14) Grigg, R.; Gunaratne, H. Q. N.; Sridharan, V. *J. Chem. Soc., Chem. Commun.* **1985**, *17*, 1183.

(15) Chimirri, A.; Grasso, S.; Romeo, G.; Zappala, M.; Fenech, G. *Heterocycles* **1985**, *23*, 895.

(16) Furutsuka, T.; Imura, T.; Kojima, T.; Kawabe, K. *Technol. Rep. Osaka Univ.* **1974**, 367.

(17) Ling, A. C.; Willard, J. E. *J. Phys. Chem.* **1968**, *72*, 1018.

(18) Hagan, T.; Pilloud, D.; Suppan, P. *Chem. Phys. Lett.* **1987**, *139*, 499.

(19) McGarry, P. F.; Doubleday, C. E., Jr.; Wu, C.-H.; Staab, H. Z.; Turro, N. J. *J. Photochem. Photobiol. A* **1994**, *77*, 109.

(20) Lewis, F. D.; Bassani, D. M.; Caldwell, R. A.; Unett, D. J. *J. Am. Chem. Soc.* **1994**, *116*, 10477.

(21) (a) Waldeck, D. H. *Chem. Rev.* **1991**, *91*, 415. (b) *Photochromism, Molecules and Systems*; Saltiel, J., Sun, Y.-P., Eds.; Elsevier: Amsterdam, 1990.